Chemical Engineering Journal 488 (2024) 150982

Contents lists available at ScienceDirect

Chemical Engineering Journal

journal homepage: www.elsevier.com/locate/cej

Versatile ionogels with tailoring performance for strain sensors, temperature alarm and self-powered wearable devices

Zhijian Zhou [a], Yongkang Bai [b,*], Longzhang Niu [b], Chunzi Lv [a], Yuqi Li [a,c,*], Lina Niu [b,*]

[a] Key Laboratory of New Processing Technology for Nonferrous Metals and Materials, Ministry of Education, College of Materials Science and Engineering, Guilin University of Technology, Guilin Guangxi 541004, China
[b] State Key Laboratory of Stomatognathic Reconstruction and Regeneration, National Clinical Research Center for Oral Diseases, School of Stomatology, The Fourth Military Medical University, Xi'an Shaanxi 710032, China
[c] Guangxi Colleges and Universities Key Laboratory of Natural and Biomedical Polymer Materials, Guangxi Department of Education, Guilin University of Technology, Guilin Guangxi 541004, China

ARTICLE INFO

Keywords:
Ionogels
Shape memory
Stretchable strain sensor
Triboelectric nanogenerator
Human-machine interaction

ABSTRACT

Ionogels with high stretchability, conductivity, self-healing and self-adhesive performances have shown great application potential in flexible electronics. In this study, a dual-crosslinked ionogel, denoted as APIx, was synthesized, showcasing versatile functionalities contingent on the ionic liquid (IL) content. Notably, API50, featuring high IL content, exhibited exceptional flexibility (1418 %) and conductivity (0.31 S m^{-1}), which conferred upon it exemplary strain-sensing performance, manifesting in rapid responsiveness (50 ms), heightened sensitivity (GF = 3.38), and whole-strain range linearity (R^2 = 0.998 at strains ranging from 10 % to 900 %). Leveraging these properties, the API50-based sensor was successfully integrated into an integrated circuit to fabricate diverse electronic devices for applications such as smart switches, signal transmission, and human–machine interaction. Conversely, ionogels with lower IL content displayed noteworthy shape memory characteristics, providing thermal responsiveness suitable for temperature alarm devices. Furthermore, these ionogels were employed to fabricate a triboelectric nanogenerator (API-TENG) exhibiting exceptional electrical output performance (134 V and 1.26 W m^{-2}). This underscores their potential in sustainable power sources and self-powered sensors for monitoring human motions. Collectively, this research introduces a novel strategy to advance the utilization of ionogels in human–machine interaction, energy harvesting devices, human healthcare, and wearable electronic devices.

1. Introduction

The rapid development of soft electronic products in diverse fields such as smart robotics [1–3], energy harvesting [4–6], and human motion monitoring [7–9], has intensified the demand for multifunctional soft conductive materials. These applications necessitate materials with exceptional stretchability and mechanical adaptability to seamlessly conform to the flexible contours of the human body [10]. Flexible strain sensors are particularly important as they convert mechanical stimuli into electrical signals. To meet future demands, strain sensors must exhibit key characteristics, including stretchability, repeatability, rapid response, wide adaptability, and high sensitivity [11]. Researchers are actively engaged in designing various types of strain sensors, exploring possibilities using soft gel materials, such as hydrogels [12,13], organogels [14,15], and ionogels [16,17]. However, hydrogels and organogels encounter challenges in dry environments, where preventing internal solvent evaporation is critical. This challenge compromises flexibility and conductivity, severely limiting their applicability in flexible electronics. In contrast, ionogels, characterized by the thermal stability and nearly zero vapor pressure of ionic liquids [18–21], emerge as a superior alternative choice.

Despite the extensive utilization of ionogels in various applications, including self-healing [22,23], transparency [24], and 3D printing [25,26], challenges persist in the multifunctional sensing domain. Numerous researchers have focused on developing strain sensors for detecting human motion [27–29]. For instance, there has been

* Corresponding authors at: Key Laboratory of New Processing Technology for Nonferrous Metals and Materials, Ministry of Education, College of Materials Science and Engineering, Guilin University of Technology, Guilin Guangxi 541004, China (Y. Li); State Key Laboratory of Stomatognathic Reconstruction and Regeneration, National Clinical Research Center for Oral Diseases, School of Stomatology, The Fourth Military Medical University, Xi'an Shaanxi 710032, China (Y. Bai, L. Niu).
E-mail addresses: yongkangbai@sina.com (Y. Bai), liyuqi@glut.edu.cn (Y. Li), niulina831013@126.com (L. Niu).

https://doi.org/10.1016/j.cej.2024.150982
Received 4 January 2024; Received in revised form 15 March 2024; Accepted 2 April 2024
Available online 3 April 2024

considerable interest in low-cost, high-performance flexible electronic device design and array integration [30–32]. However, the current strain sensors often face challenges such as high hysteresis under external forces across the entire strain range, residual strain, and real-time resistance deviation from the baseline [33]. These issues frequently lead to multiple gauge factor (GF) values within the strain range, resulting in inaccurate predictions of external deformations [34–36]. Introducing nanofillers has proven effective in addressing this concern, but an excess of fillers can create modulus differences between hydrogel matrices, impacting the sensor's response time [37–39]. A significant factor contributing to this challenge is the substantial chemical and physical property differences between most gel matrices and the conductive phase, leading to poor filler dispersion in the gel matrix [40–42]. During polymer tensile strain, inadequate dispersion and physical bond rupture result in heightened local stress, leading to alterations in Poisson's ratio and consequently impacting the material's sensing capabilities to a certain degree. Therefore, reducing the physical bonds between polymers and enhancing filler dispersion has become a challenge.

The rapid recovery of strain or resistance changes is crucial for designing wearable sensors, such as gas sensors and strain sensors. While the preservation of the resistance change is also beneficial for specific applications, such as temperature sensors and smart switches [43–45]. However, there have been few reports on integrating temperature sensors with strain sensors thus far. Nonetheless, fixing the strain change of sensors poses another challenge. Shape memory, an inherent feature in shape memory polymers, allows materials to recover from a temporary shape to a predesigned shape upon exposure to external stimuli [46,47]. This provides an ideal method for reversibly fixing the resistance change of sensors, a concept that has been scarcely reported. Nonetheless, the integration of a material with versatile functions remains a significant challenge.

In this study, we present a multifunctional ionogel (API) reinforced by ionic liquid (IL) modified zinc oxide (IMZnO). Due to its enhanced affinity and dispersion resulting from modification, IMZnO effectively enhances internal friction between molecules, leading to tighter interface bonding and improved conductivity. Additionally, the IL used as a solvent not only enhances the solubility and stability of the polymer but also avoids the occurrence of physical bonds provided by water as a solvent. Furthermore, the ionogel provides thermal stability and low volatility, enabling stable performance at high temperatures [48–52]. Meanwhile, the proportion of ionic liquids plays a pivotal role in determining the physical properties of the ionogel, thereby enabling the creation of ionogels with diverse properties tailored for specific applications. Strain sensors developed using high-IL-content ionogels demonstrated exceptional sensitivity, consistency, and reproducibility in sensing signals across extensive tensile deformations. These sensors can be integrated with circuits to create multifunctional electronic devices, including smart switches, temperature alarms, and human–machine interaction systems. Differently, ionogels with lower IL content demonstrated excellent shape memory performance, endowing the ionogel-based sensors with thermal responsiveness for application in temperature alarm devices. Additionally, ionogels as stretchable electrode materials have enabled the development of triboelectric nanogenerators (TENGs) for energy harvesting, pressure sensing, and human motion detection. This research highlights the immense potential of multifunctional ionogels in flexible sensing, rehabilitative medicine, human–machine interactions, virtual/augmented reality, and the metaverse domain.

2. Results and discussion

2.1. Preparation and characterization of API ionogels

The synthesis of multifunctional ionogels, incorporating ion-modified zinc oxide (IMZnO) and ionic liquid 1-Ethyl-3-methylimidazolium ethyl sulfate ([C_2mim][$EtSO_4$]), was achieved through a straightforward free radical polymerization process involving 2-Acrylamide-2-methylpropanesulfonic acid (AMPSA) and poly (ethylene glycol)diacrylate (PEGDA 1000) as chemical cross-linkers (Fig. 1). In the polymer cross-linked network, AMPSA serves as the main chain while PEGDA acts as the cross-linker, ensuring high elasticity and stability of the polymer segments. This polymer network, combined with the filler network formed by IMZnO, creates a dual-network structure, enhancing the conductivity and sensing performance of the polymer. As shown in Fig. 1(a), ZnO was chemically modified initially to achieve a more uniform dispersion in the ionic liquid (Figure S1), and the successful modification of ZnO can be confirmed by FTIR (Figure S2a). In Figure S2(b), peaks observed at 1569 and 1170 cm^{-1} correspond to the imidazole ring and −C = S vibration in the ionic liquid [C2mim][EtSO4] [53]. Additionally, peaks at 1112 and 1043 cm^{-1} were belong to the characteristic peaks of O = S = O, while the absorption peak at 1727 cm^{-1} signified the C = O vibration, demonstrating the copolymerization of AMPSA and PEGDA [54,55]. These findings collectively underscore the successful preparation and chemical characterization of API ionogels. As shown in Figure S3, a comparison of SEM images of ZnO and IMZnO reveals that the surface of IMZnO appears more continuous and dense than that of ZnO. This difference is attributed to the presence of a coating of an ionic liquid organic layer on the surface of IMZnO. This indicates the successful modification of IMZnO, enhancing the affinity of IMZnO particles to the polymer matrix, leading to a tighter interface bonding. Additionally, the surface of ionogel with added IMZnO appears rougher, which can strengthen the interface bonding between the IMZnO and the matrix, thereby improving the mechanical properties of APIx.

For soft gel-based sensors, exceptional mechanical properties are crucial for practical applications and the service life of ionogels in flexible devices. Hence, the ionic liquid content of ionogels, denoted as APIx (x representing the weight percent of ionic liquid), was adjusted to achieve desirable tensile performance. Fig. 2a and Figure S4 demonstrate an inverse relationship between fracture elongation and fracture strength with increasing ionic liquid content. The fracture strength decreased from 5.19 MPa to 0.11 MPa, while the fracture elongation increased from 24.8 % to 1418 % with the increasing ionic liquid content. This heightened stretchability was attributed to the plasticization of the ionic liquid, essential for the application of ionogels as soft sensors. However, excessive ionic liquid (beyond 50 %) proved detrimental to the mechanical performance of ionogels due to a decrease in the interaction between polymer chains.

The self-healing capability of ionogels is indispensable for expanding their applications and prolonging their lifespan in diverse environments. A breaking-healing test with API50, showcasing the highest stretchability, demonstrated the ability to stretch over 300 % strain again after healing at room temperature for 30 min (Fig. 2b). The healing efficiency increased with the extension of healing time, with API50 recovering 85 % of its initial mechanical strength within only 2 h (Fig. 2c and Figure S5). Beyond mechanical self-healing, electrical self-healing properties were investigated by connecting API50 into a circuit with a blue light-emitting diode (LED). The LED was lit up due to the ionic conductivity of ionogels, extinguished when the ionogel was cut into two parts, and re-lit instantly upon reconnection, demonstrating the ionogels' electrical self-healing capability (Figure S6 and Video S1). This was further validated by the resistance variation during the healing process (Fig. 2d and Figure S7), indicating repeatable healing at 25 °C or −5°C. The high healing efficiency of ionogels was attributed to abundant recyclable hydrogen bonds and ionic coordination interactions.

The ionogels also exhibited excellent antifreezing and self-adhesive performances, indispensable for the reliable application of flexible electronics. API50 maintained high flexibility at −15 °C, demonstrating its suitability as an electrode material under low-temperature conditions (Fig. 2e). Moreover, API50 exhibited strong adhesion to various substrates, with adhesive strengths onto acrylic board, aluminum tape,

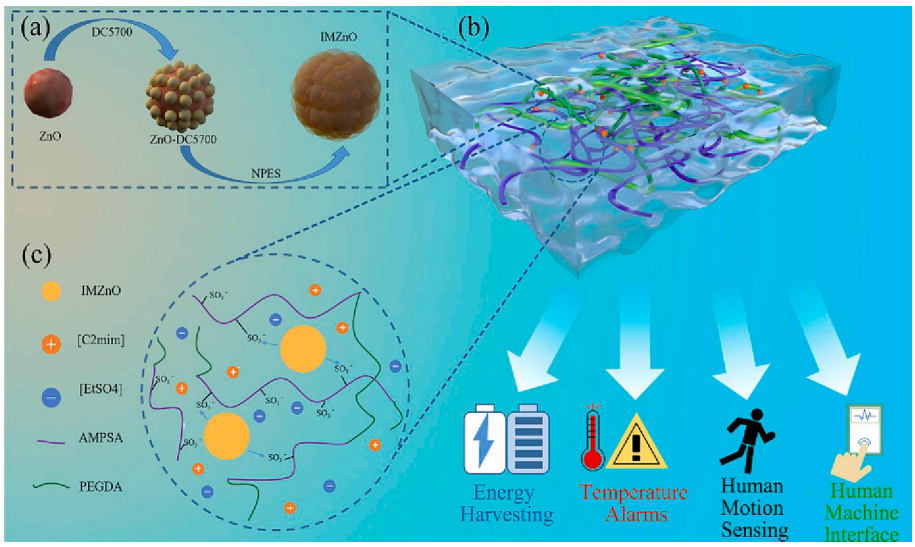

Fig. 1. (a) IMZnO synthesis process; (b) Schematic representation of the ionic gel structure; (c) Schematic illustration of internal charge in the ionogels.

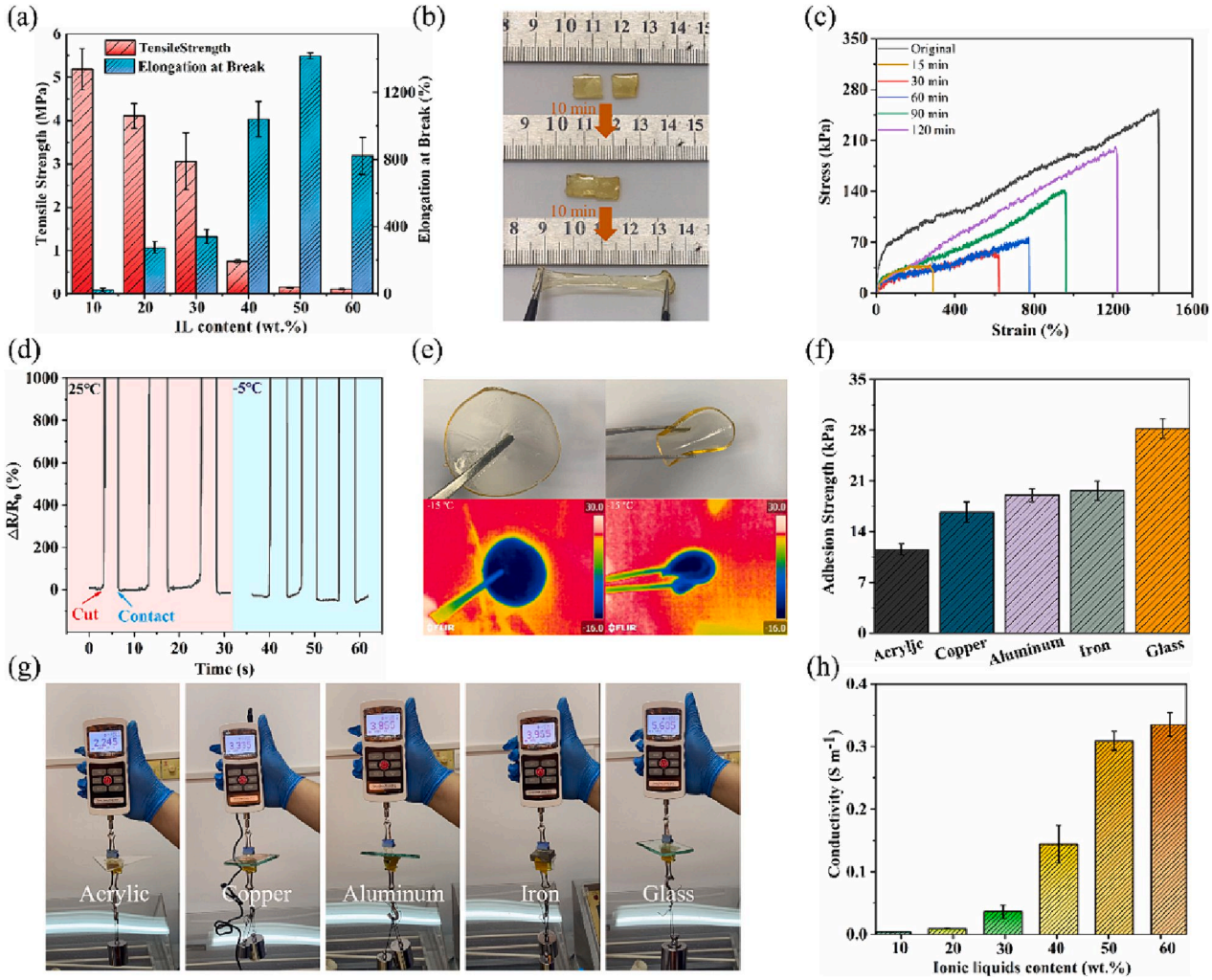

Fig. 2. (a) Mechanical properties at different ionic liquid contents; (b) images of self-healing process; (c) Stress–strain curves of API50 at different self-healing times; (d) Electrode self-healing ability at different temperatures; (e) Thermal imaging and digital photos at low temperatures; (f) Adhesion strength of API50 on different substrate materials; (g) Digital photos of adhesion strength of API50; (h) Conductivity of ionogels.

copper tape, glass, and iron block measured at 110.55, 160.68, 190.03, 190.65, and 28.21 kPa, respectively (Fig. 2f and g). This high adhesiveness was attributed to the abundant functional groups in ionogels, forming various non-covalent interactions with substrates, including hydrogen bonds, metal coordination and electrostatic interactions [56–58]. Additionally, the dynamic metal coordination bonds in the ionic gel provide a dissipation mechanism, requiring additional energy for the expansion of interface cracks.

2.2. Strain-sensing performance

In addition to flexibility, self-healing and self-adhesive characteristics, conductivity stands as a crucial parameter for wearable devices recording electrical signals. Fig. 2h and Figure S8 illustrates a positive correlation between ionic liquid content and conductivity; the maximum conductivity of API60 reached 0.35 S m^{-1}. Enhanced conductivity can be attributed to two factors: firstly, the ionic liquid acts as a solvent, facilitating the uniform dispersion of polymer chains and IMZnO in the gel, forming a more coherent conductive network structure. Secondly, an increase in ion concentration promotes ionic conductivity, enhancing the overall conductivity of ionogels.

Next, the feasibility of API50 with desirable stretchability and conductivity as strain-sensors was investigated by monitoring the real-time resistance change ($\Delta R/R_0$) under different strains. The results show that the $\Delta R/R_0$ value increased gradually with the increase of strain, and maintain consistency at a certain strain, highlighting the stable and repeatable responsiveness of the ionogel sensor to strains across a wide range from 10 % to 900 % (Fig. 3a and b). To assess the sensitivity of different sensors [59], their respective gauge factors (GF) were calculated. The results revealed that API50 exhibited a constant GF of 3.38 across the entire strain range, with a high linearity of $R^2 = 0.998$ (Fig. 3c and S9). The increased internal friction in the ionogel leads to tighter bonding between interfaces, preventing significant changes in the material's Poisson's ratio. This results in stable deformation during tensile strain, leading to a consistent relationship in resistance change. As shown in Figure S10, compared to the case without additives, the addition of IMZnO increases the loss factor, indicating an increase in internal friction with IMZnO addition [60]. So the ionogel sensor without IMZnO showed incoherent linear relationships with GF of 2.5 in the range of 0–70 % and 1.57 from 70 % to 450 % (Figure S11). This emphasizes that the physical deformation of the ionogel could be precisely detected due to the outstanding linearity of the API50-based sensor across the entire strain range. Additionally, the ionogel sensor also exhibited fast response and recovery time about 50 ms (Figure S12), which is close to that of human skin (≈100 ms) [61]. Then the long-term stability of the ionogel sensor was conducted by a consecutive 3000

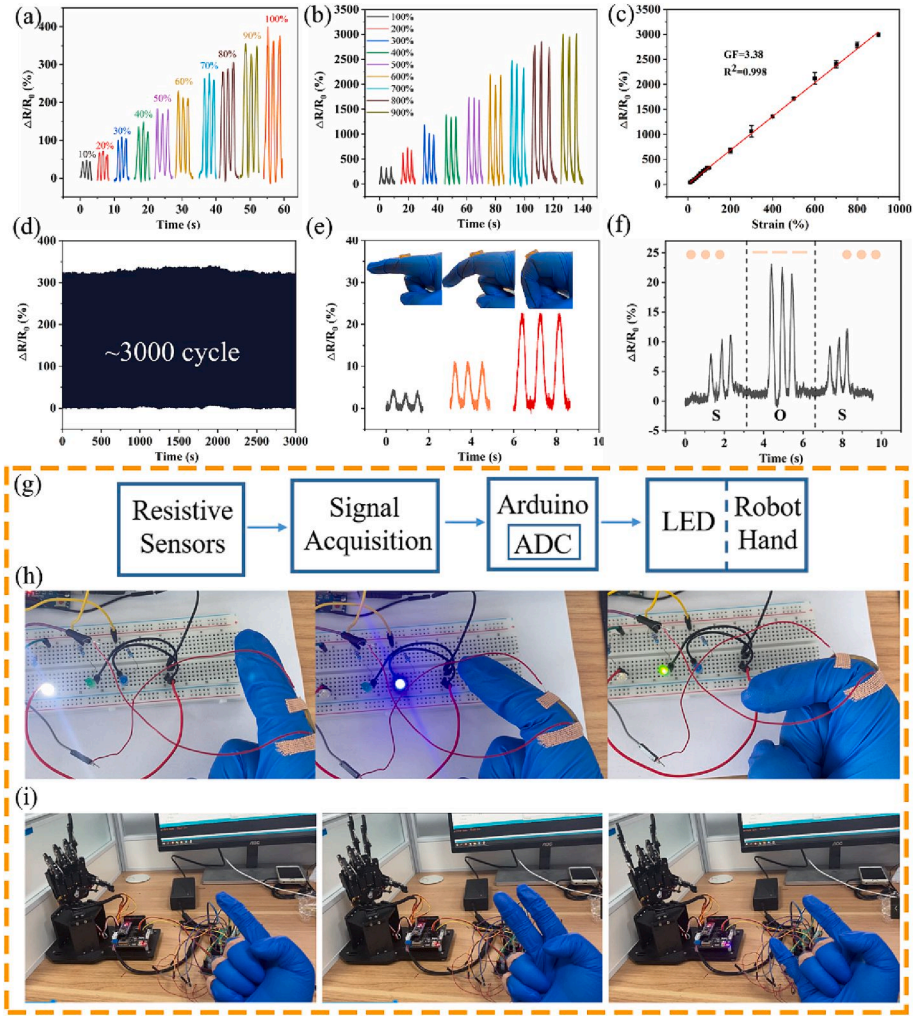

Fig. 3. (a) Relative resistance change of API50 under small strain (10–100%); (b) relative resistance change of API50 under large strain (100–900%). (c) relative resistance change of API50 under strain ranging from 10% to 900%; (d) 3000 cycles of loading–unloading tests on API50 gel at 100% strain; (e) relative resistance change at different finger bending angles; (f) schematic diagram of the integrated circuit; (g) relative resistance change under SOS Morse code; (h) illumination of different LED lights through bending fingers at various angles; (i) the control of a robotic hand through a strain sensor.

loading–unloading cycles at 100 % strain (Fig. 3d). The results showed a stable response of $\Delta R/R_0$ value of the sensor, demonstrating its outstanding stability and durability as strain sensors. Compared to previously reported gels-based sensors, the API50 sensor demonstrated exceptional flexibility, a wide detection range, high sensitivity and linearity (Table S3).

To validate the performance of API50 under extreme conditions. As shown in Figure S13a, we conducted tests on ion gels after a 2-hour self-healing process. During the testing, the change in strain sensitivity of API50 within the 0–300 % strain range after self-healing closely resembled that before self-healing. However, deviations in the GF values between the two were observed after a strain of 300 %, suggesting that the cross-section may not have fully healed. Further stretching potentially induced some minor cracks on the cross-section, affecting electronic transmission and resulting in a decrease in the corresponding GF values. Complete healing might necessitate a more extended duration. Moreover, we examined the resistance variations of API50 at distinct temperatures (Figure S13b). At 60 °C, there was a slight GF increase due to heightened molecular activity and improved movement of charge carriers, while preserving a linear correlation. However, at 80 °C, significant alterations occurred in the gel structure due to weakened intermolecular forces and increased flowability, leading to a remarkable upsurge in GF values and abrupt modifications. Subsequent assessments were carried out under diverse humidity conditions (Figure S13c). The API50 was exposed to environments with varying humidity levels for 1 h, followed by strain sensitivity testing. The results showed a decreasing trend in GF values with increasing environmental humidity. This phenomenon is ascribed to water molecules adhering to the gel surface, thereby diminishing resistance. Furthermore, in elevated humidity settings, the presence of water molecules triggered further expansion of the gel structure, resulting in reduced resistance. Consequently, as humidity rises, the gel's resistance diminishes, culminating in a GF increase.

Given the excellent sensitivity and high linearity of the API50 sensor, it can used as a strain sensor to monitor human kinematics, like finger bending (Fig. 3e). The $\Delta R/R_0$ signal increases gradually with the bending angles, enabling the distinction of finger motion. Leveraging this resistance change induced by deformation, the API50 sensor can be used in smart switches, signal transmission, and human–machine interaction. Integrated into a circuit system comprised of an Arduino microcontroller and an Analog-to-Digital Converter (ADC), the API50 sensor captures resistance changes caused by strain, converts them into changes in analog voltage values, and facilitates the realization of various applications controlled by strain change (Fig. 3f). For instance, a smart switch controlling different LED lights was devised as shown in Figure S14 and Video S2. At original state, the yellow LED was on, then it was off and the red LED was on accompanying with the stretching of API50 sensor to a specific strain (300 %) due to the increase of resistance, finally the green LED was on when the strain was over 600 %. The results demonstrated the API50 sensor can indeed be used as a multiple switch to control different LEDs by strain.

To explore the application of the API50 sensor in signal transmission, it was affixed to a finger to create an encrypted signal transmission system using Morse code to match finger bending with resistance changes. This resistance change will produce distinct analog electrical signals simultaneously to control LED lights through the multiple switches, which can be also used to transmit Morse code by light signals. For the light signals, we defined the blue light as a "dot," the green light as a "dash," and the white light as the completion of a signal transmission segment. As demonstrated in Fig. 3g and Figure S15, the API50 sensor was able to transmit short messages, such as "SOS", "WATER", and "DANGER", through finger bending according to electrical signals, while these signals also could be recognized by the change of LED lights (Fig. 3h and Video S3). The strain sensors demonstrated the capability of transmitting messages through the circuit system via electrical and light signals simultaneously, showcasing the tremendous potential of the API50 sensor in multi-channel signal communication. Moreover, the API50 sensor was employed for human–machine interaction to control robot behaviors. As depicted in Fig. 3i and Video S4, four API50 sensors were attached to the fingers and their resistance changes induced by fingers bending were collected and processed by the Arduino, subsequently sent instructions to a robotic hand for remote control. The robotic hand replicated different gestures following the change in human hand, demonstrating the application prospect of the API50 sensor in human–machine interaction and the metaverse domain.

2.3. Shape memory properties

While API50 with high ionic liquid (IL) content demonstrated excellent strain-sensing performance due to its high resilience and conductivity, the ionogels exhibited noteworthy shape memory properties when the IL content was below 20 %. Differential scanning calorimetry revealed that ionogels with IL content over 30 % possessed a glass transition temperature (T_g) below 30 °C, contributing to their high elasticity at room temperature. Conversely, when IL content decreased to 10 %, T_g increased to 85.2 °C, creating the potential for shape memory properties. (Figure S16) In the shape memory cyclic process (Fig. 4a), a straight sample was stretched to a certain strain at 100 °C (above T_g) and the temporary shape was fixed at room temperature. After that, the sample was reheated to 100 °C again to recall its original shape, and shape fixation ratio (R_f) and recovery ratio (R_r) were used to evaluated the shape memory properties. As illustrated from Table S2, all the ionogels with IL content lower than 20 % exhibit excellent shape memory performance, especially API10 with R_f and R_r both over 98 %. Utilizing this shape memory feature, API10 was employed to fabricate a temperature alarm device.

Similar to the circuit system in Fig. 3f, the API10 sensor was connected to an integrated circuit with the addition of a Bluetooth module for wireless signal transmission (Fig. 4b), and a resistance value was set as the alarm threshold. Once the resistance change reached the threshold, the red LED will be turned on and sends a warning message to the phone. The shape memory performance of API10 allowed the strain change to be fixed by the shape fixation process at room temperature, preserving the resistance change of the ionogel. Resistance changes were successfully preserved at different strains by shape fixation (Figure S17), with a high linear relationship between strain and $\Delta R/R_0$ value ensuring reliability for temperature alarm devices. As the temperature rises, the stretched API10 will recover to its original length induced by the thermal responsive shape memory effect, with its resistance change decreasing simultaneously (Figure S18 and Figure S19). Thus, the alarm system will be triggered upon the resistance reaching the threshold due to the increase of temperature. In Fig. 4C, API10 demonstrated high stability in 10 shape memory cyclic tests, maintaining almost the same resistance change after shape recovery at 100 °C. To validate the feasibility of the temperature alarm device, an alarm threshold of resistance change was set as 1000 % and its corresponding shape recovery temperature was about 80 °C according to Figure S19. Then the temperature alarm function was further demonstrated in Fig. 4d and Video S4. In the initial state, the green LED indicated normal working status with the stretched API10 sensor (75 % strain). Once the sensor was heated to 80 °C, its length contracted to about 2.4 cm, leading to the decrease of resistance change lower than the threshold of 1000 %. Subsequently, the alarm system was triggered: the red LED was lighted up, and the Bluetooth module sent a danger signal to the phone at the same time. The alarm system ceased when the sensor was stretched and fixed at room temperature again, indicating the end of the crisis. Based on the temperature alarm function of the API10 ionogel, it can be used to monitor pipeline temperature in real-time (Fig. 4e). The system issues an alert when the pipeline temperature is abnormal, signaled by the red LED and wireless signal.

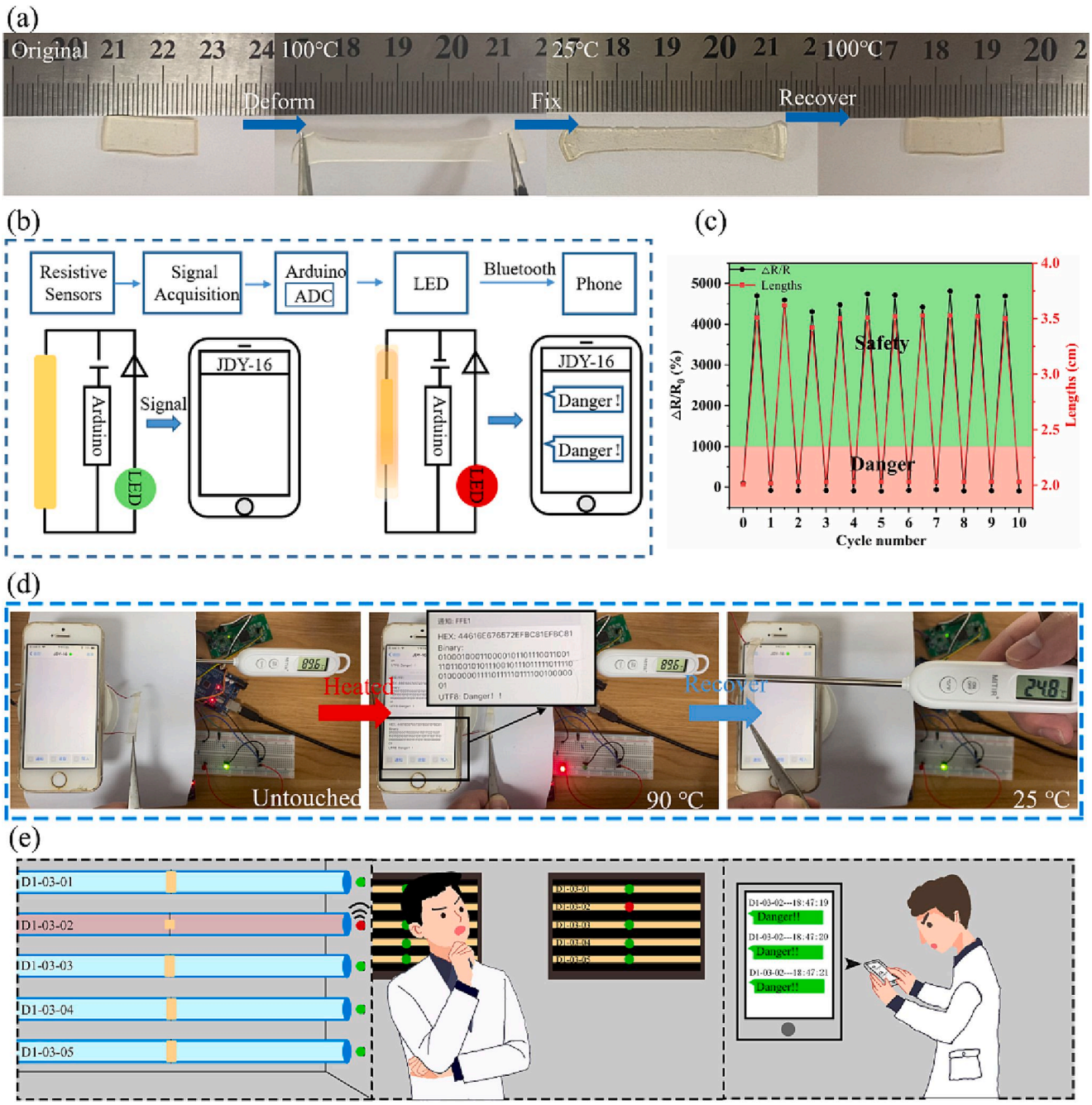

Fig. 4. (a) Shape memory performance of API10; (b) schematic diagram of using a strain sensor as a temperature alarm device; (c) relative resistance change for different lengths over 10 cyclic operations; (d) physical representation of using a strain sensor as a temperature alarm device; (e) real-time temperature prediction using the temperature alarm for industrial pipelines.

2.4. The output performance of ionogels-based TENG

In addition to the strain sensors and temperature alarm devices based on strain-resistance effect, the ionogels exhibit potential for the fabrication of triboelectric nanogenerators (TENGs) for power supply and self-powered sensors. Specifically, a sandwiched ionogel-based TENG (API-TENG) operating in single electrode mode was assembled by encapsulating ionogels into silicone. The working principle, depicted in Fig. 5a, relies on contact electrification and electrostatic induction [62,63]. In the initial state, when a nitrile glove (positive tribo-material) touches the silicone surface, equal amount positive and negative surface charges will be on the two materials due to tribo-electrification (Fig. 5a (i)). Upon separation, negative charges on the silicone surface attract positive ions within the ionogel (Fig. 5a(ii)) creating a positive ions layer at the ionogel-silicone interface. Simultaneously, negative ions accumulate at the ionogel-Cu wire interface, forming an electrical double layer [64]. (EDL) (Fig. 5a(v) and (vi)). During this process, electrons flow from the Cu wire to the ground through an external circuit until the establishment of an electrostatic equilibrium. Once the two friction materials are adequately separated, the final charge balance inhibits the continuous movement of electrons, resulting in the cessation of power generation (Fig. 5a(iii)). When the nitrile glove approaches the silicone again, this process is reversed, and the electrons will flow from the ground to the ionogel-Cu wire interface. Thus, an alternating current can be generated by the repeatable contact-separation process of the two tribo-materials.

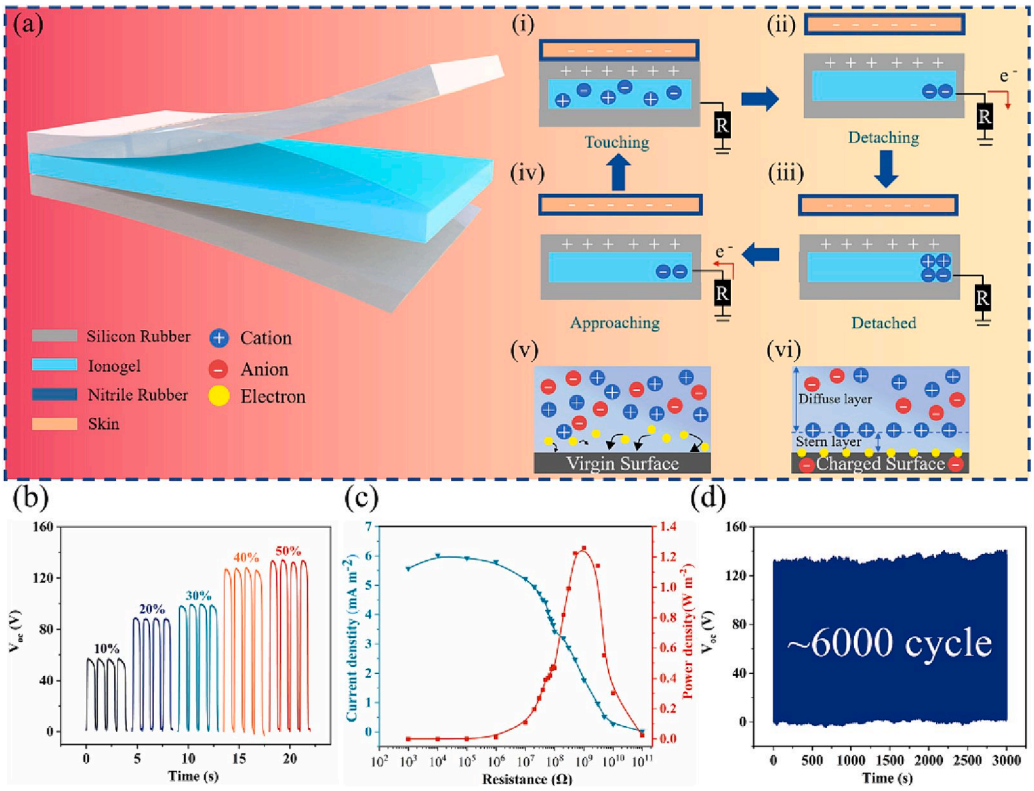

Fig. 5. (a) Working mechanism of the API-TENG; (b) open-circuit voltage at different IL content; (c) current density and power density at different resistances; (d) Open-circuit voltage after 6000 cycles.

API-TENGs with varying IL content were fabricated to explore the IL content's effect on output performance. The output performance exhibited an increasing trend with IL content, with API50-TENG demonstrating the highest output, characterized by open-circuit voltage, short-circuit current, and transferred charge values of approximately 134.3 V, 1.90 μA, and 41.74 nC, respectively (Figure S20). This specific configuration, API50-TENG, was employed in subsequent experiments. The output performance at different frequencies showed increased short-circuit current with frequency, while open-circuit voltage and transferred charge decreased slightly (Figure S21). To assess the output power of API-TENG, the current and power density were measured across varying load resistance at a frequency 1 Hz (Fig. 5c). It is clearly shown that the peak power density of the TENG is approximately 1.26 W m^{-2} when the load resistance was 100 MΩ, while the maximum current density was about 6.025 mA m^{-2}. Then the long-term stability of the API-TENG was also tested, As shown in Fig. 5d; under the condition of 2 Hz, the output voltage almost remain the same after 6000 cyclic tests, indicating the excellent stability and reliability of the API-TENG. Given that TENG devices inevitably experience various deformations in practical applications, we further tested the output

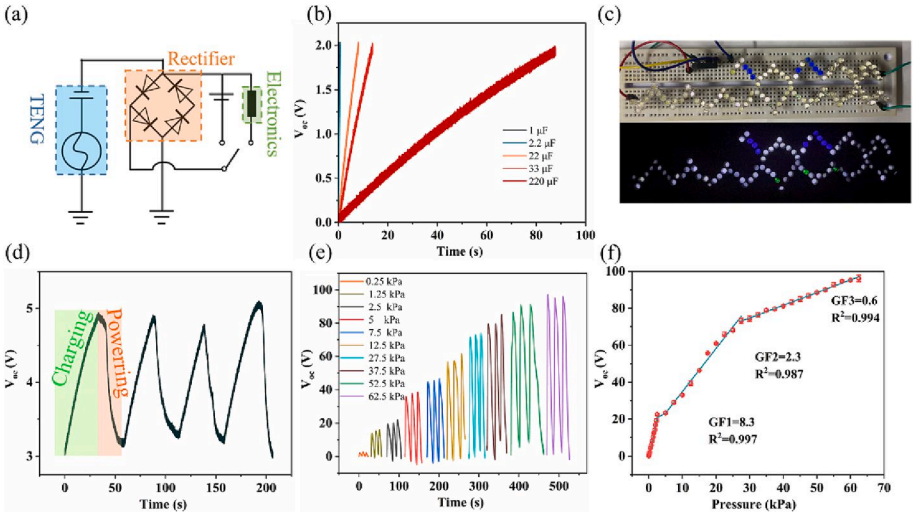

Fig. 6. (a) Equivalent circuit of the API-TENG; (b) Charging different capacitors using the API-TENG; (c) Illuminating 100 LEDs with different API-TENGs; (d) Powering LEDs with capacitors charged by the API-TENG after capacitor charging; (e) Open-circuit voltage of the API-TENG under different pressures; (f) GF corresponding to the output voltage under different pressures.

performance of the API-TENG under different strains (Figure S22). It can be found that the open-circuit voltage of API-TENG indeed decreased with the increase of strain due to the decrease of ionogel's conductivity, and it almost recovered to the raw value when the original length of the TENG was restored, demonstrating its stability and reliability after undergoing various deformations scenarios in practical applications.

The self-powered property of the API-TENG was evaluated by integrating it into a rectified circuit (Fig. 6a). The charging efficiency of the API-TENG for different commercial capacitors (1 μF, 2.2 μF, 22 μF, 33 μF, and 220 μF) was presented in Fig. 6b, and the results revealed that the charging speed decreased with the increase of capacitor capacity, while it still only took 88 s to charge the 220 μF capacitor to 2.0 V. In addition, the API-TENG could be also directly used as the power source to light 100 LEDs without reliance on other energy system, demonstrating its application as sustainable power supply (Fig. 6c and Video S6). Furthermore, utilizing the electrical storage capacity of the capacitors, the electricity generated by the API-TENG could be easily harvested, stored and drive other electronic devices at any time. As an example, a 33 μF capacitor could be charged to 5 V within 30 s by tapping the API-TENG, and the stored energy could then light up a LED for 20 s (Fig. 6d). Overall, these results indicates that the API-TENG holds great prospect as a self-powered source for various electronical applications.

The API-TENG, owing to its exceptional self-powered property, could serve as a self-powered pressure sensor for wearable electronics. The output performance of API-TENG under varying applied pressure demonstrated a positive correlation between output voltage and applied pressure across low, medium, and high-pressure regions (Fig. 6e and f). In the low-pressure region (0 to 2.5 kPa), the sensitivity reached up to 8.3 V kPa^{-1}; while it was 2.3 and 0.6 V kPa^{-1} in the medium-pressure region (2.5 to 25 kPa) and high-pressure region (25 to 62.5 kPa), respectively. These results demonstrate the exceptional performance of API-TENG self-powered sensors across various pressure ranges, showcasing unique advantages compared to previous self-powered sensors (Table S4). Based on its pressure sensing performance and high flexibility, the API-TENG functioned as a self-powered sensor for human motion monitoring. As presented in Fig. 7a–d, the API-TENG sensor was strategically attached to different joint parts including fingers, wrists, elbows, and knees, to capture biomotion signals. It is clearly shown that a voltage signal was generated and then increased accordingly with the increase of bending angles for various joints, which was attributed to the increase of pressure on the sensors. Moreover, the results also showed a high linear response behavior ($R > 0.99$ in Figure S23) between the peak voltage and bending angles, demonstrating the reliability and accuracy of the API-TENG for real-time self-powered biomotion monitoring. In addition to joint motions, the API-TENG sensor also can be employed to monitor gait motion by attaching it to the insole. As shown in Fig. 7e, the peaks voltages for walking, running and jumping activities were ~ 36 V, ~69 V, and ~ 91 V, respectively, allowing for the recognition of human motion states. This versatile application potential positions the API-TENG as a promising tool for wearable biomotion sensors in healthcare and rehabilitation.

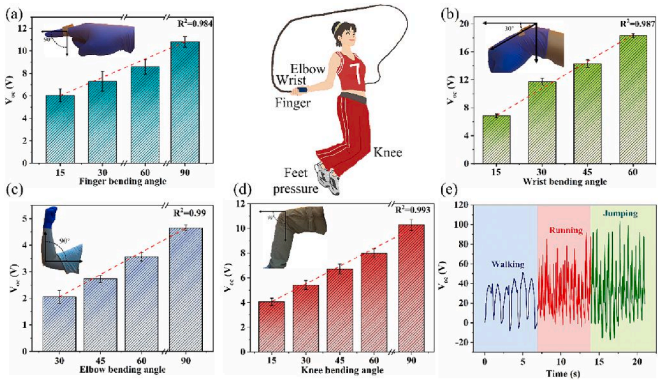

Fig. 7. Open-circuit voltage signals generated by different human motions: (a) Finger; (b) Wrist; (c) Elbow; (d) Knee; (e) Open-circuit voltage generated by different gaits.

3. Conclusion

In summary, we have developed a series of API ionogels with tunable performance for various flexible sensors depending on the IL content. The high-IL-content ionogel, API50, exhibited remarkable stretchability (1418 %), high conductivity (0.31 S m^{-1}), self-healing, anti-freezing, and self-adhesive properties. These features made it well-suited for flexible strain sensors. The API50-based strain sensors demonstrate rapid responsiveness (50 ms), excellent sensitivity (GF = 3.38), and linearity across a wide tensile strain range (10 % to 900 %). Capitalizing on its excellent strain-sensing performance, the API50 sensor can be integrated into various multifunctional electronic devices, including smart switches, signal transmission systems, and human–machine interaction circuits. Differently, the ionogels with low IL content (API10) exhibited outstanding shape memory performance with R_f and R_r both over 98 %, endowing the ionoge-based sensors with thermal responsiveness for application in temperature alarm devices. Furthermore, the ionogels are employed to fabricate ionogel-based triboelectric nanogenerators (TENGs). Among them, API50-TENG stood out with the highest output performance, including open-circuit voltage, short-circuit current, and power density values of 134 V, 1.9 μA, and 1.26 W m^{-2}, respectively, which was able to light up 100 LEDs in series. Based on its excellent self-power property, the developed API50-TENG demonstrated excellent self-powered pressure capability with a sensitivity of 8.3 V kPa^{-1}, which could serve as wearable self-powered sensors to detect various human motions with high accuracy. Therefore, this work introduces a straightforward strategy for fabricating multifunctional ionogels with strain-sensing, temperature alarming, and self-powered capabilities. The demonstrated versatility opens up promising practical applications in intelligent wearable devices, human–machine interaction, and soft robotics.

4. Experimental section

4.1. Preparation of IMZnO

Zinc oxide nanoparticles (2.1 g) were dispersed in 70 mL of deionized water through ultrasonication for 30 min. Subsequently, 30 mL of a mixture of DC5700 and methanol (DC5700: methanol = 1:2) was added, and the solution was mechanically stirred for 24 h at room temperature. The intermediate product of zinc oxide-DC5700 was then filtered, washed, and dried. After dissolving the intermediate product in dichloromethane, 10 mL of NEPS was added, and the solution was mechanically stirred for 12 h at room temperature. The resulting mixture was subjected to liquid–liquid extraction with deionized water to obtain IMZnO.

4.2. Preparation of API

A dispersion was created by mixing 1 % wt of IMZnO in 3 g of water. Subsequently, 0.8 g of PEGDA and a specific amount of 1-ethyl-3-methylimidazolium ethyl sulfate (10–60 % of the total mass) were added, followed by 30 min of ultrasonication. Next, 2.5 g of AMPSA and 0.05 g of Ammonium persulphat (APS) were added, and the mixture was mechanically stirred for 1 h. The composite hydrogel was then poured into a 60 mm culture dish and dried in an 80 °C oven for 16 h.

4.3. Materials and characterization

For convenience, the materials, instrument and detailed

characterization are available in the supporting information.

CRediT authorship contribution statement

Zhijian Zhou: Writing – original draft, Investigation, Formal analysis, Data curation, Conceptualization. **Yongkang Bai:** Writing – review & editing, Writing – original draft, Validation, Supervision, Resources, Investigation, Formal analysis, Data curation, Conceptualization. **Longzhang Niu:** Investigation, Formal analysis, Data curation. **Chunzi Lv:** Formal analysis, Data curation. **Yuqi Li:** Writing – review & editing, Supervision, Resources, Project administration, Funding acquisition, Formal analysis. **Lina Niu:** Writing – review & editing, Validation, Supervision, Resources, Funding acquisition.

Declaration of competing interest

The authors declare that they have no known competing financial interests or personal relationships that could have appeared to influence the work reported in this paper.

Data availability

Data will be made available on request.

Acknowledgements

This work was supported by National Key R&D Program of China (2022YFC2405900, 2022YFC2405901), National Natural Science Foundation of China (82325012, 81870805), the Shaanxi Key Scientific and Technological Innovation Team (2020TD-033), the Youth Innovation Team of Shaanxi Universities, and the Natural Science Foundation of Guangxi Province (2022GXNSFAA035536).

Appendix A. Supplementary data

Supplementary data to this article can be found online at https://doi.org/10.1016/j.cej.20240.150982.

References

[1] Z.Q. Shen, Z.L. Zhang, N.B. Zhang, J.H. Li, P.W. Zhou, F.Q. Hu, Y. Rong, B.Y. Lu, G. Y. Gu, High-stretchability, ultralow-hysteresis ConductingPolymer hydrogel strain sensors for soft machines, Adv. Mater. 34 (32) (2022) 2203650, https://doi.org/10.1002/adma.202203650.
[2] Z.Q. Shen, F.F. Chen, X.Y. Zhu, K. Yong, G.Y. Gu, Stimuli-responsive functional materials for soft robotics, J. Mater. Chem. B.8 (39) (2020) 8972–8991, https://doi.org/10.1039/D0TB01585G.
[3] J.W. Booth, D. Shah, J.C. Case, E.L. White, M.C. Yuen, O.C. Cyr-Choiniere, R. Kramer-Bottiglio, OmniSkins: robotic skins that turn inanimate objects into multifunctional robots, Sci. Robot. 3 (22) (2018) eaat1853, https://doi.org/10.1126/scirobotics.aat1853.
[4] J.B. Qi, A.C. Wang, W.Y. Yang, M.Y. Zhang, C.Y. Hou, Q.H. Zhang, Y.G. Li, H. Z. Wang, Hydrogel-based hierarchically wrinkled stretchable nanofibrous membrane for high performance wearable triboelectric nanogenerator, Nano Energy. 67 (2020) 104206, https://doi.org/10.1016/j.nanoen.2019.104206.
[5] W. Xu, L.B. Huang, M.C. Wong, L. Chen, G.X. Bai, J.H. Hao, Environmentally friendly hydrogel-based Triboelectric nanogenerators for versatile energy Harvesting and self-powered sensors, Adv. Energy Mater. 7 (4) (2017) 1601529, https://doi.org/10.1002/aenm.201601529.
[6] C.Z. Lv, Z.J. Zhou, Y.Q. Li, S.R. Lu, Y.K. Bai, Multi-responsive shape memory porous composites for self-powered sensors and self-sensing actuators, Chem. Eng. J. 477 (2023) 147059, https://doi.org/10.1016/j.cej.2023.147059.
[7] A. Chortos, J. Liu, Z.N. Bao, Pursuing prosthetic electronic skin, Nat. Mater. 15 (2016) 937–950, https://doi.org/10.1038/nmat4671.
[8] J.N. Kim, J. Lee, H. Lee, I.K. Oh, Stretchable and self-healable catechol-chitosan-diatom hydrogel for triboelectric generator and self-powered tremor sensor targeting at Parkinson disease, Nano Energy. 82 (2021) 105705, https://doi.org/10.1016/j.nanoen.2020.105705.
[9] Y. Deng, T. Lu, X. Zhang, Z. Zeng, R. Tao, Q. Qu, Y. Zhang, M. Zhu, R. Xiong, C. Huang, Multi-Hierarchical nanofiber membrane with typical curved-ribbon structure fabricated by green electrospinning for efficient, breathable and Sustainable air filtration, J. Membr. Sci. 660 (2022) 120857, https://doi.org/10.1016/j.memsci.2022.120857.
[10] Z.Y. Wang, M.M. Bu, K.H. Xiu, J.Y. Sun, N. Hu, L.B. Zhao, L.X. Gao, F.Z. Kong, H. Zhu, J. Song, D. Lau, A flexible, stretchable and triboelectric smart sensor based on graphene oxide and polyacrylamide hydrogel for high precision gait recognition in Parkinsonian and hemiplegic patients, Nano Energy. 104 (2022) 107978, https://doi.org/10.1016/j.nanoen.2022.107978.
[11] A.D. Qiu, P.L. Li, Z.K. Yang, Y. Yao, I. Lee, J. Ma, A path beyond metal and silicon: Polymer/Nanomaterial composites for stretchable strain sensors, Adv. Funct. Mater. 29 (17) (2019) 1806306, https://doi.org/10.1002/adfm.201806306.
[12] S. Liu, X.Y. Tian, X.S. Zhang, C.Z. Xu, L.L. Wang, Y.Z. Xia, A green MXene-based organohydrogel with tunable mechanics and freezing tolerance for wearable strain sensors, Chin. Chem. Lett. 33 (4) (2022) 2205–2211, https://doi.org/10.1016/j.cclet.2021.09.063.
[13] Z.J. Zhao, X. Fan, S.X. Wang, X.N. Jin, J.J. Li, Y.P. Wei, Y. Wang, Natural polymers-enhanced double-network hydrogel as wearable flexible sensor with high mechanical strength and strain sensitivity, Chin. Chem. Lett. 34 (6) (2023) 107892, https://doi.org/10.1016/j.cclet.2022.107892.
[14] Z.X. Zhang, L. Wang, H.T. Yu, F. Zhang, L. Tang, Y.Y. Feng, W. Feng, Highly Transparent, self-healable, and adhesive organogels for bio-inspired intelligent Ionic skins, ACS Appl. Mater. Interfaces 12 (13) (2020) 15657–15666, https://doi.org/10.1021/acsami.9b22707.
[15] A. Khan, R.R. Kisannagar, S. Mahmood, W. Chuang, M. Katiyar, D. Gupta, H. Lin, Intrinsically stretchable conductive self-healable organogels for strain, pressure, temperature, and humidity sensing, ACS Appl. Mater. Interfaces 15 (36) (2023) 42954–42964, https://doi.org/10.1021/acsami.3c08111.
[16] N. Jiang, X.H. Chang, D.W. Hu, L.R. Chen, Y.P. Wang, J.W. Chen, Y.T. Zhu, Flexible, transparent, and antibacterial ionogels toward highly sensitive strain and temperature sensors, Chem. Eng. J. 424 (2021) 130418, https://doi.org/10.1016/j.cej.2021.130418.
[17] H. Peng, F. Yang, X. Wang, E. Feng, K.J. Sun, L.L. Hao, X.S. Zhang, G.F. Ma, Rapid radiation synthesis of a flexible, self-healing, and adhesive Ionogel with environmental tolerance for multifunctional strain sensors, ACS Appl. Mater. Interfaces. 15 (44) (2023) 51763–51773, https://doi.org/10.1021/acsami.3c12082.
[18] K.D. Semavin, N.S. Chilingarov, O.B. Dorofeeva, E.V. Skokan, D.A. Kalinyuk, V. Y. Markov, Evaporation and thermal decomposition of 1-ethyl-3-methylimidazolium chloride, J. Mol. Liq. 380 (2023) 121733, https://doi.org/10.1016/j.molliq.2023.121733.
[19] X.Y. Li, M.K. Yan, J. Xiao, H.L. Lian, Ultrafast fabrication of deep eutectic solvent flexible Ionic gel with high-transmittance, freeze-resistant and conductivity by frontal Polymerization, J. Colloid Interface Sci. 650 (2023) 1382–1392, https://doi.org/10.1016/j.jcis.2023.07.038.
[20] S.S. Lingala, Ionic-liquid-based nanofluids and their heat-transfer applications: a comprehensive review, ChemPhysChem. 24 (22) (2023) e202300191.
[21] S. Hao, T. Li, X. Yang, H. Song, Ultrastretchable, adhesive, fast self-healable, and three-dimensional printable photoluminescent Ionic skin based on hybrid network Ionogels, ACS Appl. Mater. Interfaces. 14 (1) (2022) 2029–2037, https://doi.org/10.1021/acsami.1c21325.
[22] M. Qi, R.Q. Yang, Z. Wang, Y.T. Liu, Q.C. Zhang, B. He, K.W. Li, Q. Yang, L. Wei, C. F. Pan, M.X. Chen, Bioinspired self-healing soft electronics, Adv. Funct. Mater. 33 (17) (2023) 2214479, https://doi.org/10.1002/adfm.202214479.
[23] M. Zhu, J. Yu, Z. Li, B. Ding, Self-healing fibrous membranes, Angew. Chem. Int. Ed. 61 (41) (2022) e202208949.
[24] S.F. Xiang, X.J. He, F. Zheng, Q.H. Lu, Multifunctional flexible sensors based on Ionogel composed Entirely of Ionic liquid with long alkyl chains for enhancing mechanical properties, Chem. Eng. J. 439 (2022) 135644, https://doi.org/10.1016/j.cej.2022.135644.
[25] H. Nulwala, A. Mirjafari, X. Zhou, Ionic liquids and Poly[Ionic liquid]s for 3D printing – a focused mini-review, Eur. Polym. J. 108 (2018) 390–398, https://doi.org/10.1016/j.eurpolymj.2018.09.023.
[26] Y.H. Ma, D.Z. Zhang, Z.H. Wang, H. Zhang, H. Xia, R.Y. Mao, H.L. Cai, H.X. Luan, Self-adhesive, anti-freezing MXene-based hydrogel strain sensor for motion monitoring and handwriting recognition with deep Learning, ACS Appl. Mater. Interfaces 15 (24) (2023) 29413–29424, https://doi.org/10.1021/acsami.3c02014.
[27] J.F. Xia, L. He, Z.L. Lu, L.P. Liu, J.N. Song, S.Y. Chen, Q.S. Wang, F.A. Hammad, Y. L. Tian, Stretchable and sensitive strain sensors based on CB/MWCNTs–TPU for human motion capture and health monitoring, ACS Appl. Nano Mater. 6 (11) (2023) 9736–9745, https://doi.org/10.1021/acsanm.3c01447.
[28] R.Y. Yang, H.Z. Song, Z. Zhou, S.D. Yang, X. Tang, J.K. He, S.Y. Liu, Z.P. Zeng, B. R. Yang, X.C. Gui, Ultra-sensitive, multi-directional flexible strain sensors based on an MXene film with periodic wrinkles, ACS Appl. Mater. Interfaces 6 (15) (2023) 8345–8354, https://doi.org/10.1021/acsami.2c22158.
[29] J. Zhang, E. Liu, S. Hao, X. Yang, T. Li, C. Lou, M. Run, H. Song, 3D printable, ultra-stretchable, self-healable, and self-adhesive dual cross-linked nanocomposite Ionogels as ultra-durable strain sensors for motion detection and Wearable human-machine Interface, Chem. Eng. J. 431 (2022) 133949, https://doi.org/10.1016/j.cej.2021.133949.
[30] Y. Ma, Y. Gao, L. Liu, X.Y. Ren, G.H. Gao, Skin-contactable and antifreezing strain sensors based on bilayer hydrogels, Chem. Mater. 32 (20) (2020) 8938–8946, https://doi.org/10.1021/acs.chemmater.0c02919.
[31] D. Sun, Y.F. Feng, S.C. Sun, J. Yu, S.Y. Jia, C. Dang, X. Hao, J. Yang, W.F. Ren, R. C. Sun, C.Y. Shao, F. Peng, Transparent, self-adhesive, conductive organohydrogels with fast gelation from lignin-based self-catalytic system for extreme environment-resistant Triboelectric nanogenerators, Adv. Funct. Mater. 32 (28) (2022) 2201335, https://doi.org/10.1002/adfm.202201335.

[32] D. Wang, D. Zhang, P. Li, Z. Yang, Q. Mi, L. Yu, Electrospinning of flexible poly (vinyl Alcohol)/MXene nanofiber-based humidity sensor self-powered by monolayer molybdenum diselenide piezoelectric nanogenerator, Nano-Micro Lett. 13 (1) (2021) 57, https://doi.org/10.1007/s40820-020-00580-5.
[33] D. Wang, D. Zhang, Y. Yang, Q. Mi, J. Zhang, L. Yu, Multifunctional latex/polytetrafluoroethylene-based Triboelectric nanogenerator for self-powered organ-like MXene/Metal–Organic framework-derived CuO nanohybrid ammonia sensor, ACS Nano. 15 (2) (2021) 2911–2919, https://doi.org/10.1021/acsnano.0c09015.
[34] D. Wang, D. Zhang, M. Tang, H. Zhang, F. Chen, T. Wang, Z. Li, P. Zhao, Rotating Triboelectric-electromagnetic nanogenerator driven by tires for self-powered MXene-based flexible Wearable electronics, Chem. Eng. J. 446 (2022) 136914, https://doi.org/10.1016/j.cej.2022.136914.
[35] Y.M. Ni, X.R. Zang, J.J. Chen, T.X. Zhu, Y. Yang, J.Y. Huang, W.L. Cai, Y.K. Lai, Flexible MXene-based hydrogel enables Wearable human-computer Interaction for intelligent underwater communication and sensing rescue, Adv. Funct. Mater. 33 (2023) 2301127, https://doi.org/10.1002/adfm.202301127.
[36] D.M. Zhong, Y.H. Xiang, Z.C. Wang, Z. Chen, J.J. Liu, Z.L. Wu, R. Xiao, S.X. Qu, W. Yang, A visco-Hyperelastic model for hydrogels with tunable water content, J. Mech. Phys. Solids. 173 (2023) 105206, https://doi.org/10.1016/j.jmps.2023.105206.
[37] M.H. Khalili, C.J. Williams, C. Micallef, F. Duarte-Martinez, A. Afsar, R. Zhang, S. Wilson, E. Dossi, S.A. Impey, S. Goel, A.I. Aria, Nanoindentation response of 3D printed PEGDA hydrogels in a hydrated environment, ACS Appl. Polym. Mater. 5 (2) (2023) 1180–1190, https://doi.org/10.1021/acsapm.2c01700.
[38] X. Gao, M.P. Zheng, X.D. Yan, J. Fu, M.K. Zhu, Y.D. Hou, The alignment of BCZT Particles in PDMS boosts the sensitivity and cycling reliability of a flexible piezoelectric touch sensor, J. Mater. Chem. c. 7 (4) (2019) 961–967, https://doi.org/10.1039/C8TC04741C.
[39] A.K. Zachariah, A.K. Chandra, P.K. Mohammed, J. Parameswaranpillai, S. Thomas, Experiments and modeling of non-Linear viscoelastic responses in natural rubber and chlorobutyl rubber nanocomposites, Appl. Clay Sci. 123 (2016) 1–10, https://doi.org/10.1016/j.clay.2016.01.004.
[40] Y. Jiang, Z.Y. Liu, N. Matsuhisa, D.P. Qi, W.R. Leow, H. Yang, J.C. Yu, G. Chen, Y. Q. Liu, C.J. Wan, Z.J. Liu, X.D. Chen, Auxetic mechanical metamaterials to enhance sensitivity of stretchable strain sensors, Adv. Mater. 30 (12) (2018) 1706589, https://doi.org/10.1002/adma.201706589.
[41] D. Li, J. Yuan, Q.Y. Cheng, P. Wei, G.J. Cheng, C.Y. Chang, Additive printing of recyclable anti-counterfeiting patterns with sol-gel cellulose nanocrystal inks, Nanoscale. 13 (27) (2021) 11808–11816, https://doi.org/10.1039/D1NR01777B.
[42] S.P. Mao, S.H. Zeng, Z.Y. Li, X.B. Han, J.Y. Yu, Effects of solvent-free bentonite fluid on physical, rheological and aging properties of SBS modified bitumen, Case Stud. Constr. Mater. 19 (2023) e02590.
[43] D.M. Wilson, Electronic Interface circuits for resistance-based sensors, IEEE Sens. J. 22 (11) (2022) 10223–10234, https://doi.org/10.1109/JSEN.2021.3124766.
[44] W.Y. Choi, J.H. Kwon, Y.M. Kim, H.C. Moon, Multimodal Wearable Ionoskins enabling independent recognition of external stimuli without crosstalk, Small. 19 (37) (2023) 2301868, https://doi.org/10.1002/smll.202301868.
[45] L.R. Chen, Y.Q. Xu, Y.F. Liu, J. Wang, J.W. Chen, X.H. Chang, Y.T. Zhu, Flexible and Transparent electronic skin sensor with sensing capabilities for pressure, temperature, and humidity, ACS Appl. Mater. Interfaces. 15 (20) (2023) 24923–24932, https://doi.org/10.1021/acsami.3c03829.
[46] W. Lu, X.X. Le, J.W. Zhang, Y.J. Huang, T. Chen, Supramolecular shape memory hydrogels: a new bridge between stimuli-responsive Polymers and Supramolecular chemistry, Chem. Soc. Rev. 46 (5) (2017) 1284–1294, https://doi.org/10.1039/C6CS00754F.
[47] S. Mondal, Temperature responsive shape memory polyurethanes, Polym.-Plast. Technol. Mater. 60 (14) (2021) 1491–1518, https://doi.org/10.1080/25740881.2021.1906903.
[48] W.Q. Liao, X.K. Liu, Y.Q. Li, X. Xu, J.X. Jiang, S.R. Lu, D.Q. Bao, Z. Wen, X.H. Sun, Transparent stretchable, temperature-stable and self-healing Ionogel-based Triboelectric nanogenerator for biomechanical energy collection, Nano Res. 15 (3) (2022) 2060–2068, https://doi.org/10.1007/s12274-021-3797-x.
[49] Y.L. Verma, M.P. Singh, R.K. Singh, Effect of ultrasonic irradiation on Preparation and properties of Ionogels, J. Nanomater. (2012) e570719.
[50] D. Meghnani, H. Gupta, S.K. Singh, N. Srivastava, R. Mishra, R.K. Tiwari, A. Patel, A. Tiwari, R.K. Singh, Fabrication and electrochemical Characterization of lithium metal battery using IL-based Polymer electrolyte and ni-rich NCA cathode, Ionics. 26 (10) (2020) 4835–4851, https://doi.org/10.1007/s11581-020-03656-9.
[51] A.K. Gupta, R.K. Singh, S. Chandra, Studies on mesoporous silica Ionogels Prepared by sol-gel method at different gelation temperatures, RSC Adv. 3 (33) (2013) 13869–13877, https://doi.org/10.1039/C3RA41774C.
[52] S.K. Shalu, R.K. Chaurasia, S. Singh, Chandra, thermal stability, complexing behavior, and Ionic transport of Polymeric gel membranes based on Polymer PVdF-HFP and Ionic liquid, [BMIM][BF4], J. Phys. Chem. b. 117 (3) (2013) 897–906, https://doi.org/10.1021/jp307694q.
[53] M.P. Singh, R.K. Singh, S. Chandra, Ionic liquids confined in porous matrices: physicochemical properties and applications, Prog. Mater. Sci. 64 (2014) 73–120, https://doi.org/10.1016/j.pmatsci.2014.03.001.
[54] S. Çavuş, Poly[Methacrylamide-co-2-Acrylamido-2-Methyl-1-propanesulfonic acid] hydrogels: investigation of pH- and temperature-dependent swelling Characteristics and their Characterization, J. Polym. Sci. Part B Polym. Phys. 48 (23) (2010) 2497–2508, https://doi.org/10.1002/polb.22152.
[55] X.M. Xing, L.W. Li, T. Wang, Y.W. Ding, G.M. Liu, G.Z. Zhang, A self-healing Polymeric material: from gel to plastic, J. Mater. Chem. a. 2 (29) (2014) 11049–11053, https://doi.org/10.1039/C4TA02079K.
[56] X.R. Zhang, Q.J. Fu, Y.C. Wang, H.N. Zhao, S.W. Hao, C. Ma, F. Xu, J. Yang, Tough liquid-free Ionic conductive Elastomers with robust adhesion and self-healing properties for Ionotronic Devices, Adv. Funct. Mater. (2023) 2307400, https://doi.org/10.1002/adfm.202307400.
[57] J.W. Yang, R.B. Bai, B.H. Chen, Z.G. Suo, Hydrogel adhesion: a Supramolecular synergy of chemistry, topology, and mechanics, Adv. Funct. Mater. 30 (2) (2020) 1901693, https://doi.org/10.1002/adfm.201901693.
[58] X.L. Lyu, H.Q. Zhang, S.C. Yang, W.Q. Zhan, M.M. Wu, Y. Yu, Z.H. Shen, Z.G. Zou, Strain-stiffening Ionogel with high-temperature tolerance via the synergy of Ionic clusters and hydrogen bonds, ACS Appl. Mater. Interfaces. 15 (26) (2023) 31888–31898, https://doi.org/10.1021/acsami.3c05802.
[59] W.T. Zhu, F. Qiu, C.X. Xiong, S.K. Song, Polymeric Ion functionalized graphite nanoplatelets with flowability, Mater. Res. Express. 5 (8) (2018) 085013, https://doi.org/10.1088/2053-1591/aad36a.
[60] H. Zhang, D. Zhang, B. Zhang, D. Wang, M. Tang, Wearable pressure sensor Array with layer-by-layer assembled MXene Nanosheets/Ag nanoflowers for motion monitoring and human-machine Interfaces, ACS Appl. Mater. Interfaces. 14 (43) (2022) 48907–48916, https://doi.org/10.1021/acsami.2c14863.
[61] R.S. Johansson, J.R. Flanagan, Coding and use of tactile signals from the fingertips in object manipulation tasks, Nat. Rev. Neurosci. 10 (5) (2009) 345–359, https://doi.org/10.1038/nrn2621.
[62] Z.N. Zhang, N. Yin, Z.S. Wu, S.H. Pan, D.A. Wang, Research methods of contact electrification: theoretical simulation and Experiment, Nano Energy. 79 (2021) 105501, https://doi.org/10.1016/j.nanoen.2020.105501.
[63] G. Zhu, B. Peng, J. Chen, Q.S. Jing, Z.L. Wang, Triboelectric nanogenerators as a new energy technology: from fundamentals, Devices, to applications, Nano Energy. 14 (2015) 126–138, https://doi.org/10.1016/j.nanoen.2014.11.050.
[64] S.Q. Lin, L. Xu, A. Chi Wang, Z.L. Wang, Quantifying electron-transfer in liquid-solid contact electrification and the formation of electric double-layer, Nat. Commun. 11 (1) (2020) 399, https://doi.org/10.1038/s41467-019-14278-9.